Front. Earth Sci. 2024, 18(2): 347–363
https://doi.org/10.1007/s11707-022-1046-6

RESEARCH ARTICLE

Dynamic synthetic analysis of circulation field of tropical cyclones affecting Shanghai

Wen GU[1], Caijun YUE (✉)[2], Zhihui HAN[1], Yanqing GAO[1], Yuqi TANG[1], Xiangyu AO[3,4], Yao YAO[2]

1 Shanghai Ecological Forecasting & Remote Sensing Center, Shanghai 200030, China
2 Shanghai Marine Meteorological Centre, Shanghai 200030, China
3 Shanghai Typhoon Institute, China Meteorological Administration, Shanghai 200030, China
4 Key Laboratory of Numerical Modeling for Tropical Cyclone (China Meteorological Administration), Shanghai 200030, China

Abstract Eleven tropical cyclones (TCs) affected Shanghai and crossed the same latitude as Shanghai from 2007 to 2018. According to similar tracks from best-track data, TCs that cause significant precipitation in Shanghai can be divided into three types: landfall TCs, nearshore northward TCs, and western TCs. Based on ERA5 reanalysis data, the dynamic synthesis method was used to synthesize TC circulation situations to compare thermal, dynamic, water vapor, and stability conditions within TC circulations during the period when they affected Shanghai. The conclusions are as follows. 1) When the three TC types are at the same latitude as Shanghai, they are all in the divergent field in the upper troposphere. For the landfall type, the subtropical high at 500 hPa is stronger and farther north than usual, and there is a high-pressure dam on the north side of the TCs. 2) The warm advection of the three TC types at 925 hPa is located in the northern quadrant of the TCs. The dynamic and water vapor conditions are good in the north-western quadrant of landfall and western TCs, and more favorable in the eastern quadrant of nearshore northward TCs. 3) The favorable effects of all three types on precipitation in Shanghai come from the boundary layer. Water vapor, upward motion, and instability conditions of landfall TCs are superior to the other two TC types. The best water vapor, dynamic, and convective instability conditions are at the northern boundary in Shanghai during landfall TCs, and the main sources of water vapor in Shanghai come from the eastern and northern boundaries. During nearshore northward TCs, the main contribution to precipitation is from the eastern boundary, while better dynamic and water vapor conditions come from the western and northern boundaries during western TCs. The above findings provide scientific and technical support for operational forecasting precipitation from TCs affecting mega-cities.

Keywords tropical cyclones, dynamic synthetic analysis, ERA5 reanalysis, Shanghai, similar track

Received February 10, 2022; accepted June 27, 2022

E-mail: yuecaijun2000@163.com

1 Introduction

China is one of the countries most affected by tropical cyclones (TCs), with more than 10 TCs per year on average (Feng et al., 2013). TCs can cause catastrophic weather such as gales, rainstorms, and storm surges, as well as secondary disasters such as landslides and mudslides, endangering people's lives and property and causing huge losses to the national economy (Chen and Ding, 1979; Lei et al., 2009). Therefore, understanding the evolution of TCs is crucial in order to prevent and mitigate disasters.

Many studies on TCs with similar evolutionary features have used synthetic analysis methods based on circulation background fields to reveal the key factors causing the evolutionary features (Frank, 1977; Gray, 1979; Yu et al., 2013; Feng et al., 2014; Yin et al., 2016). Frank (1977) pointed out that averaging multiple TC situation field information synthetically according to the absolute spatial position would cause smoothing. Gray (1979) proposed a dynamic synthesis method that follows TCs which solves the smoothing problem. Shou and Yao (1995) used the center of a TC as the coordinates of the origin and conducted a diagnostic analysis of the synthetic environmental fields of "explosive" and "slow-varying" TCs. Li et al. (2004, 2005) used the dynamic synthesis method following TCs based on NCEP reanalysis data to study the differences in environmental field characteristics that lead to the long-term maintenance and rapid disappearance of landfall TCs. Dong et al. (2010)

conducted a dynamic diagnosis and analysis of the differences between the large-scale circulation characteristics of landfall TCs with steeply increasing and gentle precipitation. Qian et al. (2013) studied the differences and similarities in the situational and physical fields of nearshore steering and landfall tracks based on European Centre for Medium-Range Weather Forecasts (ECMWF) ERA-40 and ERA-Interim reanalysis data. Ni et al. (2013) found that the main cause of abrupt changes in TC tracks in the north-west Pacific is the east–west oscillation of subtropical high pressure. Using NCEP FNL reanalysis data and CMORPH precipitation data, Bu and Li (2020) compared and analyzed differences in the atmospheric circulation field, vertical shear of ambient horizontal winds, and dynamic and thermal conditions within typhoon circulation that caused left-side and right-side precipitation of landfall TCs in east China. All of the above studies yielded meaningful results, but careful analysis reveals that they are mainly based on reanalysis information with a temporal resolution of 6 h and a spatial resolution of 1°. Thus, there is still room for further improvement in terms of spatial and temporal variability.

Recently, the ECMWF released the ERA5 reanalysis data, which has a temporal resolution of 1 h and a spatial resolution of 0.25°. Many scholars have assessed the applicability of this data to China. Meng et al. (2018) found that these data had a higher correlation with the observed reality in China than ERA-Interim data, particularly with regard to significant improvements in relative humidity and wind field in the lower troposphere. Belmonte Rivas and Stoffelen (2019) determined that ERA5 is superior to ERA-Interim in terms of mean wind and transient wind errors as well as wind divergence. Using ERA5 reanalysis data, Li et al. (2021) studied the spatial and temporal distribution of wave fields and the wind–wave growth relationship of TCs affecting the Bohai Sea. Bian et al. (2021) determined that the size distribution characteristics of TCs in the North Pacific based on ERA5 reanalysis data were closer to the observed values than other reanalysis data. Huang et al. (2021) investigated the reasons for the differences in rainfall areas in Fujian caused by TC Soulik (2013) and TC Trami (2018) based on ERA5 reanalysis data. The above research shows that ERA5 reanalysis data, with its higher spatial and temporal resolution, can be used to study the evolutionary characteristics of TCs in detail. However, according to our analysis, these studies did not include research on TCs affecting mega-cities.

Shanghai is a coastal mega-city that experiences an average of 2.4 TCs per year (Shi et al., 2013). There is significant interannual variation in the frequency of TCs affecting Shanghai, with the possibility of up to six and as few as none in any given year. Xu (2005) analyzed the influence of TCs with similar tracks on Shanghai winds, and found that their influence on wind direction depended on their location relative to Shanghai, and their influence on wind speed distribution depended on their intensity and on suburban differences, thus showing that regular patterns exist in the influence of TCs on wind speed and wind direction in Shanghai. Yue et al. (2019) discovered that obstruction due to urbanization significantly affects the local precipitation distribution of TCs in Shanghai. Previous studies noted that the impact of TCs on wind and rainfall in Shanghai has both universal laws and regional differences, but most studies are still limited to the impact of a single TC, which is not representative. In operational forecasting, TCs with similar tracks are used as an important tool for predicting the evolution characteristics and storm impacts of current TCs, but there are few comparative studies on the characteristics of TC circulation and the dynamic, thermal, and water vapor conditions closely related to precipitation under the influence of different TC types with similar tracks in Shanghai.

In this study, best-track data were used to divide TCs affecting Shanghai during 2007–2018 into landfall, nearshore northward, and western types. Based on ERA5 reanalysis data, the dynamic synthesis method was used to synthesize TC circulation situations to compare their thermal, dynamic, water vapor, and stability conditions during the period when they affected Shanghai. Total helicity diagnostic analysis was also conducted. The purpose was to analyze the similarities and differences of TC circulation and meteorological factors that trigger the precipitation of different TC types affecting Shanghai and to provide a scientific basis for the prevention and mitigation of TC disasters in Shanghai. The research results can also provide scientific and technological support for accurate prediction of TC precipitation and fine services in other coastal megacities. The rest of the paper is organized as follows. The data introduction, synthesis and diagnostic methods, and TC overview are given in Section 2. In Section 3, the circulation background and synoptic field of three TC categories are investigated. We discuss the comprehensive diagnostic analysis of three TC types circulation in Section 4. The relevant conditions and sources conducive to precipitation in Shanghai are discussed in Section 5. The conclusions are given in Section 6.

2 Data and methodology

2.1 Data

In this paper, tropical cyclone (TC) is a collective term for tropical storm, severe tropical storm, typhoon, strong typhoon, and super typhoon, and a general term for storms of different magnitudes. A TC is considered to affect Shanghai if at least one automatic station in Shanghai has a maximum wind speed of ⩾ 8 magnitude

(17.0 m·s^{-1}), 10 min of mean maximum wind speed ⩾ 6 magnitude (10.8 m·s^{-1}), and process rainfall of ⩾ 50 mm (Xu, 2005; Shi et al., 2013). In this study, only TCs that caused significant precipitation in Shanghai and cross the same latitude as Shanghai were selected for the sample.

ERA5 reanalysis data were released in 2016, providing a temporal resolution of 1 h, horizontal spatial resolution of 0.25°, and 281 meteorological elements (including geopotential height, temperature, pressure, wind, and humidity) of 37 isobaric layers (Hersbach et al., 2020). Recent studies of the worldwide applicability of ERA5 reanalysis data have shown that the quality of these data are generally better than that of other reanalysis data such as ERA-Interim and MERRA-2 (Albergel et al., 2018; Meng et al., 2018; Belmonte Rivas and Stoffelen, 2019; Bian et al., 2021).

The best-track data used in the present study is the Northwest Pacific (NWP) TC track information released by the Shanghai Typhoon Institute (STI), which has a temporal resolution of 6 h (Lu et al., 2021). Studies have shown that the STI best-track data are highly reliable for information on TC tracks and intensity affecting China (Lei, 2001; Song et al., 2010). To match the 1 h temporal resolution of ERA5 reanalysis data, the 6 h best-track data were first linearly interpolated to hour-by-hour, and then the closest point in ERA5 reanalysis data was determined, based on the hour-by-hour latitude and longitude of the TC center, to be the TC center of the reanalysis field.

2.2 Dynamic synthesis of TC circulation field

Based on the best-track information, the tracks of TCs affecting Shanghai were grouped into three categories: 1) TCs that directly land in Shanghai (landfall type); 2) TCs that proceed northward on the sea and remain to the east of Shanghai (nearshore northward type); and 3) TCs that continue to go north after landing in the south of Shanghai, and locate to the west when at the same latitude as Shanghai (western type). Eleven TCs that affected Shanghai from 2007 to 2018 were recovered: four landfall type, three nearshore northward type, and four western type. The details are shown in Table 1.

The coordinates of longitude and latitude at the center of a TC at time t are x_t and y_t, thus the position of the TC is at (x_t, y_t). The time when the TC is at the same latitude as Shanghai (31.3°N) is denoted as t_0; 6, 12, and 18 h before the TC is at the same latitude as Shanghai are denoted as t_{-6}, t_{-12}, and t_{-18}, respectively; and 6, 12, and 18 h after the TC is at the same latitude as Shanghai are denoted as t_{+6}, $t_{+12,}$, and t_{+18}, respectively. First, we refer to the dynamic circulation background synthesis method used by Bu and Li (2020) in their study of landfall TCs in east China. The latitude and longitude coordinates of TC centers for the same type at the same time are arithmetically averaged, and the result is used as the latitude and longitude coordinates of a synthesized TC center on similar tracks. Taking the landfall type TCs in Table 1 as an example, the synthesized latitude and longitude coordinates at the same latitude as Shanghai (time t_0) are as follows:

$$\overline{x_{t_0}} = \frac{1}{4}(x_{t_0,1818} + x_{t_0,1812} + x_{t_0,1810} + x_{t_0,1416}), \quad (1)$$

$$\overline{y_{t_0}} = \frac{1}{4}(y_{t_0,1818} + y_{t_0,1812} + y_{t_0,1810} + y_{t_0,1416}). \quad (2)$$

Then, the translations of the original TCs relative to the synthesized TCs at time t_0 are calculated, and the overall translational fields of different meteorological elements, such as temperature, pressure, wind, and humidity, are arithmetically averaged. The resulting average meteorological element field is the synthetic background circulation field of landfall type TCs at time t_0. The

Table 1 Summary of TCs affecting Shanghai from 2007 to 2018

Type	Number of TC	Name of TC	TCs at same latitude as Shanghai		
			GMT (YYYYMMDDHH)	Air pressure/ hPa	Near-center wind speed/ (m· s^{-1})
Landfall	1818	Rumbia	2018081703	984	23
	1812	Jongdari	2018080308	993	17
	1810	Ampil	2018072203	980	28
	1416	Fung-wong	2014092306	998	18
Nearshore northward	1509	Chan-hom	2015071118	970	35
	1109	Muifa	2011080619	968	34
	1007	Kompasu	2010090103	958	45
Western	1814	Yagi	2018081303	992	18
	1614	Meranti	2016091604	1002	15
	0908	Morakot	2009081018	995	20
	0713	Wipha	2007091915	996	19

synthetic background circulation fields of the other two TC types are obtained similarly. In addition, the circulation range in this study is centered on a TC with a diameter of 8 latitude/longitude distances (≈450 km).

It is noteworthy that, unlike in the work of Bu and Li (2020), the arithmetic average of latitudes and longitudes of the center of each TC type in this study is defined as the location of the synthesized TC. The purpose is to study the influence of TCs with similar tracks in Shanghai, so that the actual base map is preserved, which makes the analysis results have practical application value.

2.3 Introduction to diagnostic analysis methods

In this study, temperature advection, wind field divergence, water vapor flux and divergence, and total helicity diagnostic analyses were performed. Specific descriptions are given below.

2.3.1 Temperature advection

Temperature advection is the horizontal movement of warm and cold air. Warm advection raises the temperature, and warm advection in the lower troposphere enhances instability. The equation for temperature advection is as follows:

$$-\vec{V}\cdot\nabla T=-\left(u\cdot\frac{\partial T}{\partial x}+v\frac{\partial T}{\partial y}\right), \tag{3}$$

where T represents temperature, and u and v represent east–west and north–south wind speeds, respectively. The other notations are physical quantities commonly used in meteorology.

2.3.2 Wind field divergence

Wind field divergence is a physical quantity of the intensity of wind convergence and divergence. Because the vertical divergence in the atmosphere is much smaller than the horizontal divergence, meteorological wind field divergence usually refers to horizontal wind field divergence. The convergence of wind fields in the lower troposphere causes upward motion. The equation for horizontal wind field divergence is

$$D=\frac{\partial u}{\partial x}+\frac{\partial v}{\partial y}, \tag{4}$$

where u and v represent east–west and north–south wind speeds, respectively. The other notations are physical quantities commonly used in meteorology.

2.3.3 Water vapor flux and divergence

Water vapor flux is the mass of water vapor flowing per unit of time through a unit cross-sectional area orthogonal to the velocity vector, and the direction of the water vapor flux is the direction of the velocity. The equation for horizontal water vapor flux is

$$\vec{F}=\frac{q\cdot\vec{V}}{g}=\frac{1}{g}(uq\vec{i}+vq\vec{j}), \tag{5}$$

where q represents the specific humidity, which is the ratio of the mass of water vapor to the total mass of air (in g/g or g/kg), g is the gravitational acceleration, and u and v represent east–west and north–south wind speeds, respectively. The other notations are physical quantities commonly used in meteorology.

Water vapor flux divergence usually refers to horizontal water vapor flux divergence, which is the amount of water vapor imported or lost horizontally per unit time and unit volume. Water vapor flux convergence means an increase in water vapor, which is beneficial to precipitation. The equation for horizontal water vapor flux is

$$A=\nabla\cdot\left(\frac{1}{g}\cdot\underset{V}{\rightarrow}\cdot q\right)=\frac{1}{g}\left(\frac{\partial uq}{\partial x}+\frac{\partial vq}{\partial y}\right), \tag{6}$$

where the notation definitions are the same as those for water vapor flux.

2.3.4 Total helicity

Helicity is a physical quantity that represents the movement of fluid along the rotation direction while rotating, and its magnitude reflects the strength of rotation movement along the rotation axis (Yue et al., 2011). A TC is a weather system with strong helicity. Increased helicity will inhibit the dissipation and diffusion of nonlinear energy in a TC, allowing it to develop or maintain (Tan and Wu, 1994). Helicity is defined as the volume fraction of the point product of wind speed and vorticity. The total helicity of the P coordinate system is calculated as follows:

$$H=\vec{V}\cdot\nabla\times\vec{V}=\left(\frac{\partial\omega}{\partial y}-\frac{\partial v}{\partial P}\right)u+\left(\frac{\partial u}{\partial P}-\frac{\partial\omega}{\partial x}\right)v+\left(\frac{\partial v}{\partial x}-\frac{\partial u}{\partial y}\right)\omega, \tag{7}$$

where u, v, and ω represent latitudinal, longitudinal, and vertical velocity, respectively. The other notations are physical quantities commonly used in meteorology.

2.4 Overview of TCs affecting Shanghai

Four landfall type TCs have affected Shanghai (Fig. 1(a)). Among them, TCs Rumbia (No. 1818), Jongdari (No. 1812), and Fung-wong (No. 1416) landed on the south coast and Ampil (No. 1810) landed at Chongming Island in northeast Shanghai. All four TCs reached their

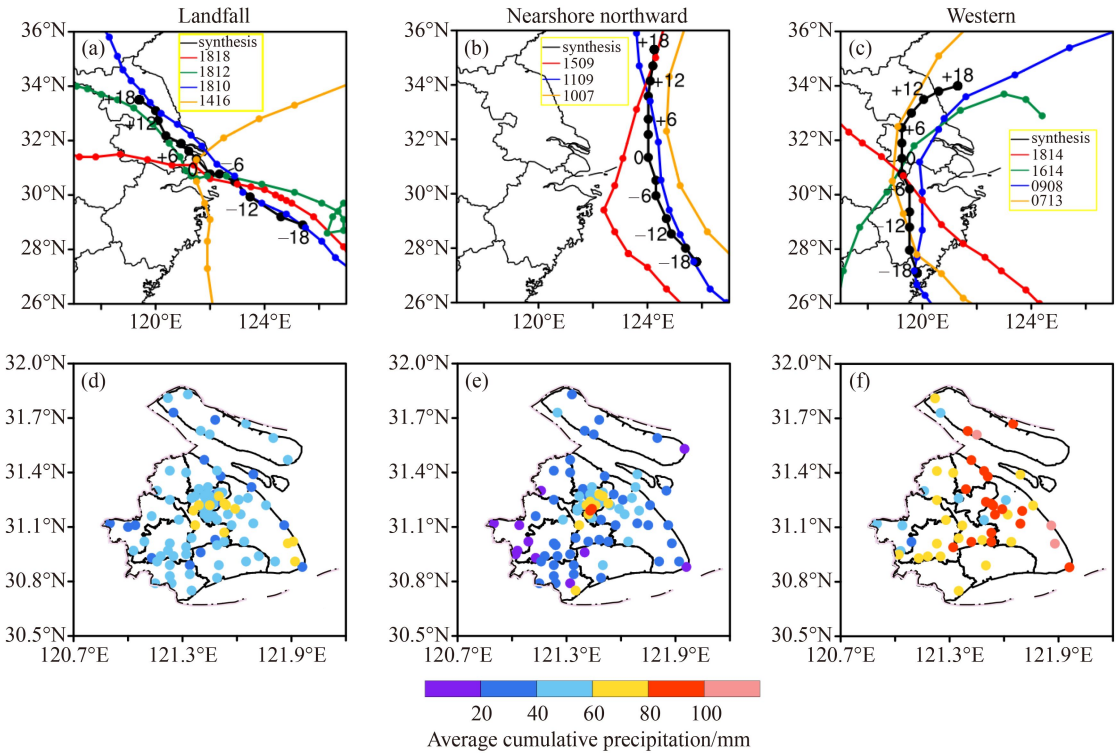

Fig. 1 (a)–(c) TC and synthetic TC tracks, and (d)–(f) average cumulative precipitation (dots, unit: mm) of three TC types. Left column, landfall type; middle column, nearshore northward type; right column, western type.

strongest level before arriving at the same latitude as Shanghai. The average intensity of landfall type TCs when they are at the same latitude as Shanghai is between that of nearshore northward and western type TCs (Table 1). The synthetic track of landfall type TCs moves north-westward at the same latitude as Shanghai, with the landing point on the east coast of the city. Figure 1(d) shows the average rainfall of landfall type TCs in Shanghai, with cumulative rainfall ranging from 24.4 to 69.0 mm.

Three nearshore northward type TCs affected Shanghai (Fig. 1(b)). Of the three, TC Chan-hom (No. 1509) was the closest and TC Kompasu (No. 1007) was the farthest. The average intensity of nearshore northward TCs is the strongest among the three types, and TCs Cham-hom and Kompasu were nearly at their strongest level when they affected Shanghai. The synthetic track of nearshore northward type TCs is mainly northward before and after reaching the same latitude as Shanghai, with the closest distance approximately 210 km from the city over the East China Sea. Figure 1(e) shows the average rainfall of nearshore northward TCs in Shanghai; the rainfall amount is between 6.0 and 99.8 mm, with great spatial distribution differences.

Four western TCs affected Shanghai (Fig. 1(c)). TC Yagi (No. 1814) and TC Wipha (No. 0713) landed in Zhejiang Province, and TC Meranti (No. 1614) and TC Morakot (No. 0908) landed in Fujian Province. The average intensity of western type TCs is weaker than that of landfall and nearshore northward type TCs at the same latitude as Shanghai. The synthetic track of western type TCs is mainly northward after landing. At the same latitude, TCs are about 190 km west of Shanghai. Figure 1(f) shows the average rainfall of western type TCs, with cumulative rainfall ranging from 39.9 to 133.3 mm.

The above analysis shows that all three types of TCs have caused significant precipitation in Shanghai. The average cumulative rainfall of western type TCs is the highest among the three types, and the average intensity of nearshore northward type TCs is the strongest when the TCs are at the same latitude as Shanghai.

3 Background circulation analysis of the three TC types

Figure 2 shows the synthesized temperature, geopotential height, and wind fields of the three types of TCs at 200 and 500 hPa at the same latitude as Shanghai. As shown in Fig. 2(a), for the landfall type, the South Asia high at 200 hPa of the landfall type is located on the Tibetan Plateau. The subtropical high at 200 hPa is located in eastern China and the East China Sea, with stronger intensity and a farther westward position compared to normal conditions. The TC is in the divergent field near the center of the subtropical high. For the nearshore northward type, the South Asia high at 200 hPa is zonally distributed (Fig. 2(b)), located in southern China and the

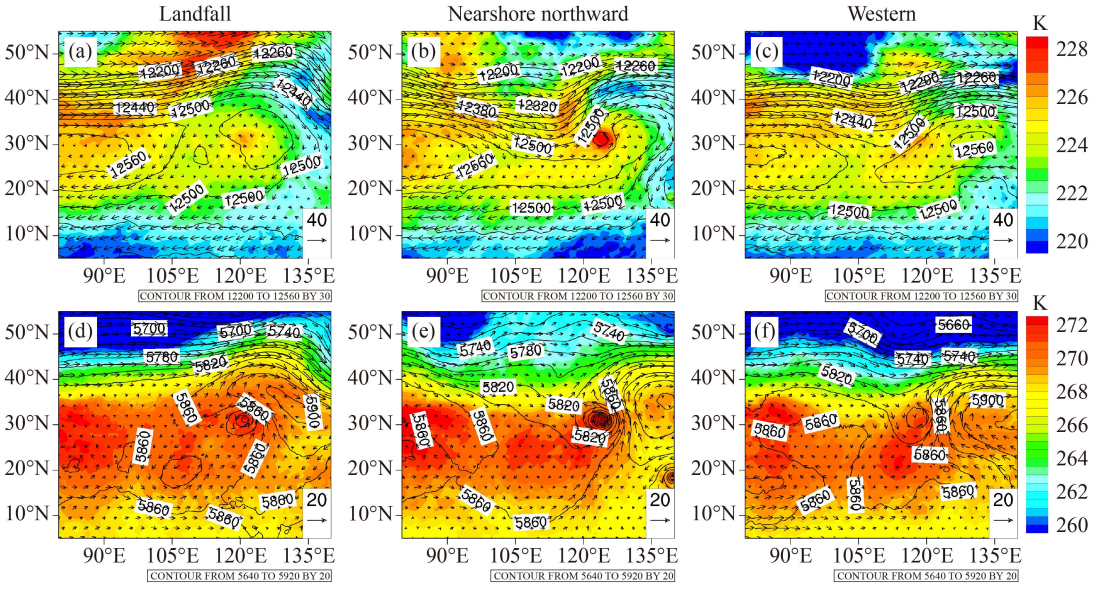

Fig. 2 Background circulation of three TC types at same latitude as Shanghai at (a)–(c) 200 hPa and (d)–(f) 500 hPa. Temperature (color shading, unit: K), geopotential height (solid line, unit: gpm), and wind field (vector, unit: $m \cdot s^{-1}$). Left column, landfall type; middle column, nearshore northward type; right column, western type.

northern Indo-China Peninsula, with weaker intensity and a farther southward position. The subtropical high at 200 hPa is located over southern Japan more eastward than usual. North China is controlled by a trough, with a wide range and strong intensity. The nearshore northward type TC is located in the divergent field east of the trough and west of the subtropical high. The warm core structure of the TC is clear and significant, indicating strong intensity. Figure 2(c) shows that for the western type, the South Asia high at 200 hPa is located in the south-west of the Tibetan Plateau with a farther south-westward position. The subtropical high pressure is zonally distributed and located in south-eastern China and the East China Sea. North China is controlled by a trough. The TC is located in the south-west flow ahead of the trough with a blurred warm core structure, indicating weak intensity.

As shown in Fig. 2(d), the landfall type TC circulation at 500 hPa has a clearly warm core structure. The subtropical high is zonally distributed from north-west to south-east. A high-pressure dam lies on the north side of the TC. The nearshore northward type TC at 500 hPa has a significant warm core with the strongest mean intensity among the three TC types (Fig. 2(e)). The subtropical high pressure is located over Japan with a farther north-eastward position. The TC lies on the western side of the subtropical high and is affected by southerly flow. As illustrated in Fig. 2(f), the circulation of the western type TC at 500 hPa is loose. The warm core structure of the TC was damaged, indicating that it was transitioning into an extratropical cyclone. The subtropical high lies over southern Japan. A cold trough is located in northern China and the TC lies the south of the trough with cold air involved in its circulation.

In general, when the three TC types are at the same latitude as Shanghai, they are located in the divergent field at 200 hPa. The difference is that for the landfall type, the South Asia high and subtropical high are stronger and located farther northward, and the TCs lie near the center of the subtropical high. For the nearshore northward and western types, the South Asia high is weaker and located farther southward than usual. Moreover, the subtropical high is located quite eastward, and there is a trough in northern China. The TCs lie between the trough and the subtropical high. At 500 hPa, there is a high-pressure dam on the north side the landfall type TC, while the nearshore northward and western type TCs are located in the west of the subtropical high.

4 Comprehensive diagnostic analysis of the circulation of three types of TCs

A diagnostic analysis of the vertical profile of the synthetic meteorological field (Section 5) reveals that the thermal and dynamic conditions and water vapor transport of the TCs mainly originate from the boundary layer. Therefore, the 925 hPa synthetic meteorological field was selected as the study object in this section. In addition, since this study focused on the influence of TCs on Shanghai, the moment when the three types of TCs are the closest to Shanghai was chosen. This section provides the diagnostic analysis results of TCs at the same latitude as Shanghai, and the impact of TCs over a longer period of time is shown in Section 5.

4.1 Analysis of temperature advection

At 925 hPa, there is warm advection in the central and

northern quadrants of landfall TCs (Fig. 3(a)), which increases instability and is conducive to the development of cloud systems. In contrast, there is cold advection in the southern quadrant, which is unfavorable to cloud development. The northern quadrant near the center of a nearshore northward TC has warm advection, but the eastern and southern quadrants have cold advection (Fig. 3(b)). The northern and eastern quadrants of western TCs have warm advection, while the south-western quadrant has weak cold advection (Fig. 3(c)).

Overall, there is warm advection at 925 hPa in the northern quadrant of all three TC types. This is due to easterly winds transporting warm advection to the TC from the warm sea surface, which increases instability and cloud development on the northern side of the TC. There is cold advection in the southern quadrant of all three TC types, which is associated with westerly winds transporting cold advection from the mainland to the southern side of the TC circulation. The difference is that nearshore northward TCs have stronger cold and warm advection than the other two TC types, which is due to the high wind speed of their circulation. When the three TC types cross the same latitude as Shanghai, the city is controlled by the warm advection of TC circulation, which leads to low-level warming and reduced stability, causing cloud development and precipitation.

4.2 Wind field divergence analysis

At 925 hPa, the landfall TC is dominated by wind field convergence, which occurs only at the center, indicating the downdraft flow at the center of the TC (Fig. 3(d)). The intensity of wind field convergence in the western quadrant of the TC exceeds 5.0×10^{-5} s^{-1}, which is favorable to cloud development at this location. The center of the nearshore northward TC has wind field divergence, while the area near the center of TC circulation has strong wind convergence (Fig. 3(e)). The strongest wind convergence is located in the eastern quadrant of the TC, and the intensity is more than −1.0

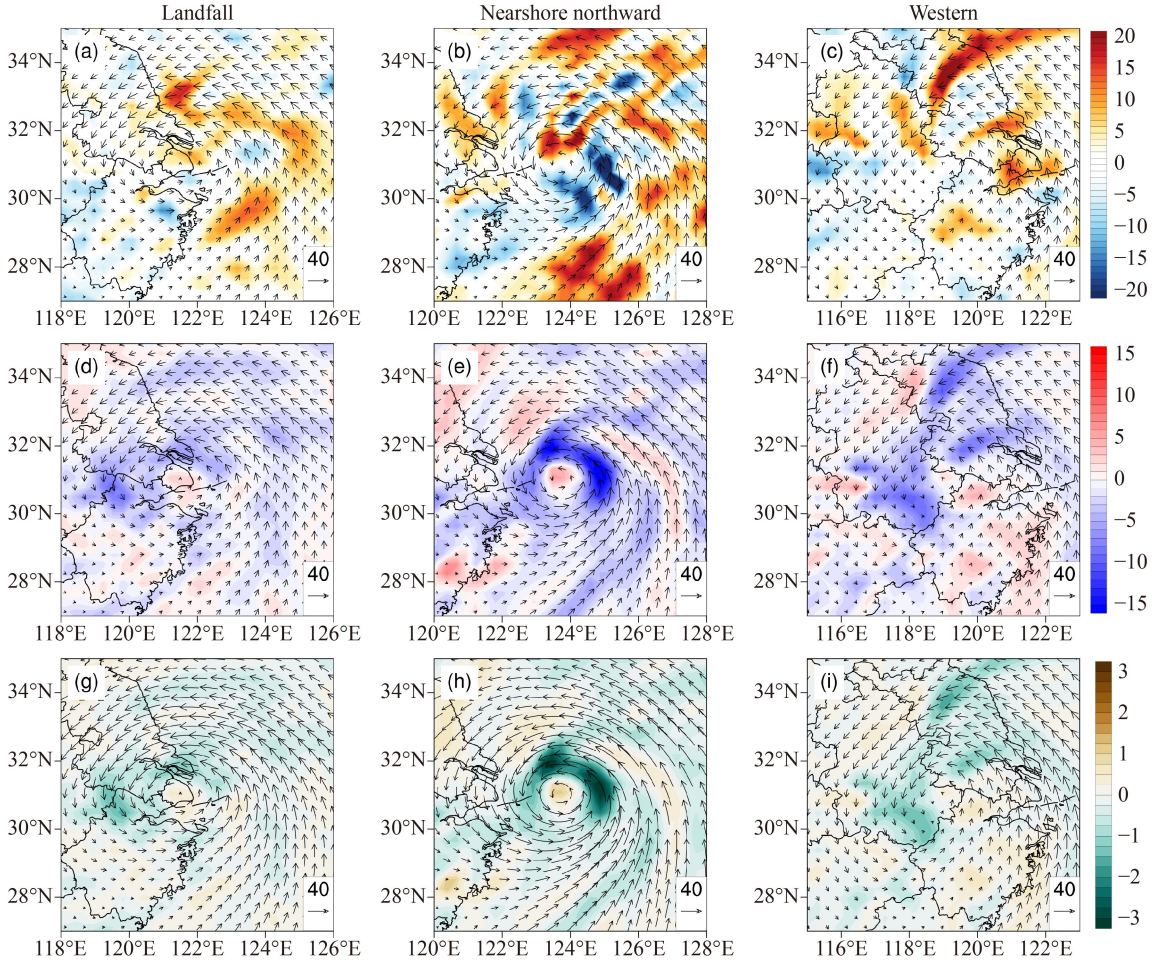

Fig. 3 Three types of TCs at same latitude as Shanghai at 925 hPa: (a)–(c) temperature advection (color shading, unit: 10^{-5} K·s^{-1}) and wind field (vector, unit: m·s^{-1}); (b)–(f) wind field divergence (color shading, unit: 10^{-5} ·s^{-1}) and wind field (vector, unit: m·s^{-1}); (g)–(i) water vapor flux (vector, unit: g·cm^{-1}·hPa^{-1}·s^{-1}) and water vapor flux divergence (color shading, unit: 10^{-7} g·cm^{-2}·hPa^{-1}·s^{-1}). Left column, landfall type; middle column, nearshore northward type; right column, western type.

$\times 10^{-4}$ s^{-1}, indicating that there is strong upward movement to promote cloud development. Wind field divergence is not evident at the center of the western TC, due to the filling of the its center after it lands (Fig. 3(f)). The convergence area of the western TC wind field is located in the northern and western quadrants, and the intensity exceeds -6.0×10^{-5} s^{-1}.

In conclusion, at 925 hPa, landfall and nearshore northward TCs have wind field divergence at their centers, and wind field convergence is dominant within a radius of 250 km from near the centers. The difference is that the wind convergence area is located in the northern and western quadrants of landfall TCs, the eastern quadrant of nearshore northward TCs, and the northern and western quadrants of western TCs. Nearshore northward TCs have stronger wind field convergence than the other two TC types due to their high wind speed. When landfall TCs cross the same latitude as Shanghai, the city is at the center, where the wind field is divergent, but with nearshore northward and western TCs there is no significant wind field convergence in Shanghai.

4.3 Analysis of water vapor conditions

At 925 hPa, the center of landfall TCs has water vapor flux divergence, which is not conducive to precipitation (Fig. 3(g)). The northern and western quadrants of TCs have water vapor flux convergence with intensity above 1.0×10^{-7} $g \cdot cm^{-2} \cdot hPa^{-1} \cdot s^{-1}$, which is conducive to precipitation. For nearshore northward TCs, except the center, the circulation shows strong water vapor flux convergence with intensity exceeding 3.0×10^{-7} $g \cdot cm^{-2} \cdot hPa^{-1} \cdot s^{-1}$. The eastern and northern quadrants have high water vapor flux convergence, which is beneficial to heavy precipitation (Fig. 3(h)). The western and northern quadrants of western TCs have water vapor flux convergence with intensity above 1.0×10^{-7} $g \cdot cm^{-2} \cdot hPa^{-1} \cdot s^{-1}$, which is favorable to precipitation (Fig. 3(i)). However, the southeast quadrant has water vapor flux divergence, which is not conducive to precipitation.

In conclusion, the near central region of the circulation of three types of TCs is dominated by water vapor flux convergence at 925 hPa, which is conducive to precipitation. The difference is that the water vapor flux convergence of landfall and western type TCs is located in the northern and western quadrants. The intensity of water vapor flux convergence of nearshore northward TCs is the strongest among the three types, because TCs located at sea have sufficient water vapor supply. When landfall TCs cross the same latitude as Shanghai, the city is at the center, with water vapor flux divergence, but there is no significant water vapor flux convergence with nearshore northward and western TCs.

The above analysis shows that when the three TC types are at the same latitude as Shanghai, warm advection is located in the northern quadrant at 925 hPa. Areas of wind field convergence and water vapor flux convergence are located near the center of all three TC types, which is favorable to rainfall. The difference is that dynamic and water vapor conditions are better in the western and northern quadrants of landfall and western TCs, while they are better in the eastern quadrant of nearshore northward TCs. Nearshore northward TCs have stronger temperature advection, dynamics, and water vapor convergence than the other two TC types due to their high speed. When the three TC types are at the same latitude as Shanghai, the city is affected by warm advection at 925 hPa, but the dynamics and water vapor conditions are ordinary. The horizontal distribution characteristics of precipitation-related factors for the three TC types were analyzed, and the characteristics in the vertical direction are given in Section 5.

5 Analysis of conditions related to precipitation in Shanghai

When the three TC types are close to the same latitude as Shanghai, the city is within the circulation of each one. In this section, the Shanghai boundary is divided into four sections: northern, eastern, southern, and western boundaries. The average of meteorological elements of four grids from each boundary are used as boundary representatives to examine the different characteristics of the time-altitude evolution of precipitation-related factors at the four boundaries, so as to reveal the source of precipitation differences in Shanghai caused by the three TC types (Fig. 4). The physical quantities include humidity, water vapor flux and divergence, stability, and vertical velocity. The time period is 24 h, including before and after the TC reaches the same latitude as Shanghai.

5.1 Relative humidity

When landfall TCs affect Shanghai, the relative humidity

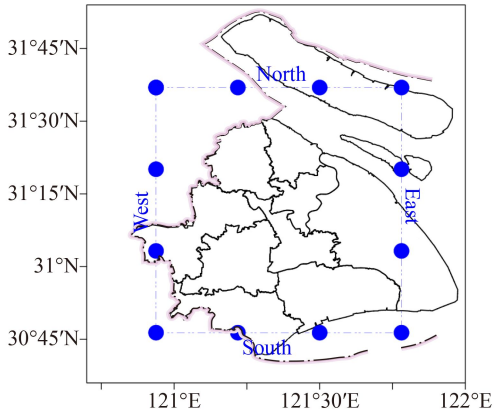

Fig. 4 Locations of four boundaries and grids in Shanghai.

at the boundary layer and lower troposphere of the four boundaries is nearly saturated (Figs. 5(a), 5(d), 5(g), 5(j)). The northern boundary has the longest duration of water vapor saturation (21 h) and the deepest saturation zone, which starts 9 h before the TC is at the same latitude as Shanghai and lasts until 12 h after it passes that latitude. The saturated layer thickness exceeds 500 hPa from 3 h before to 3 h after the TC is at the same latitude

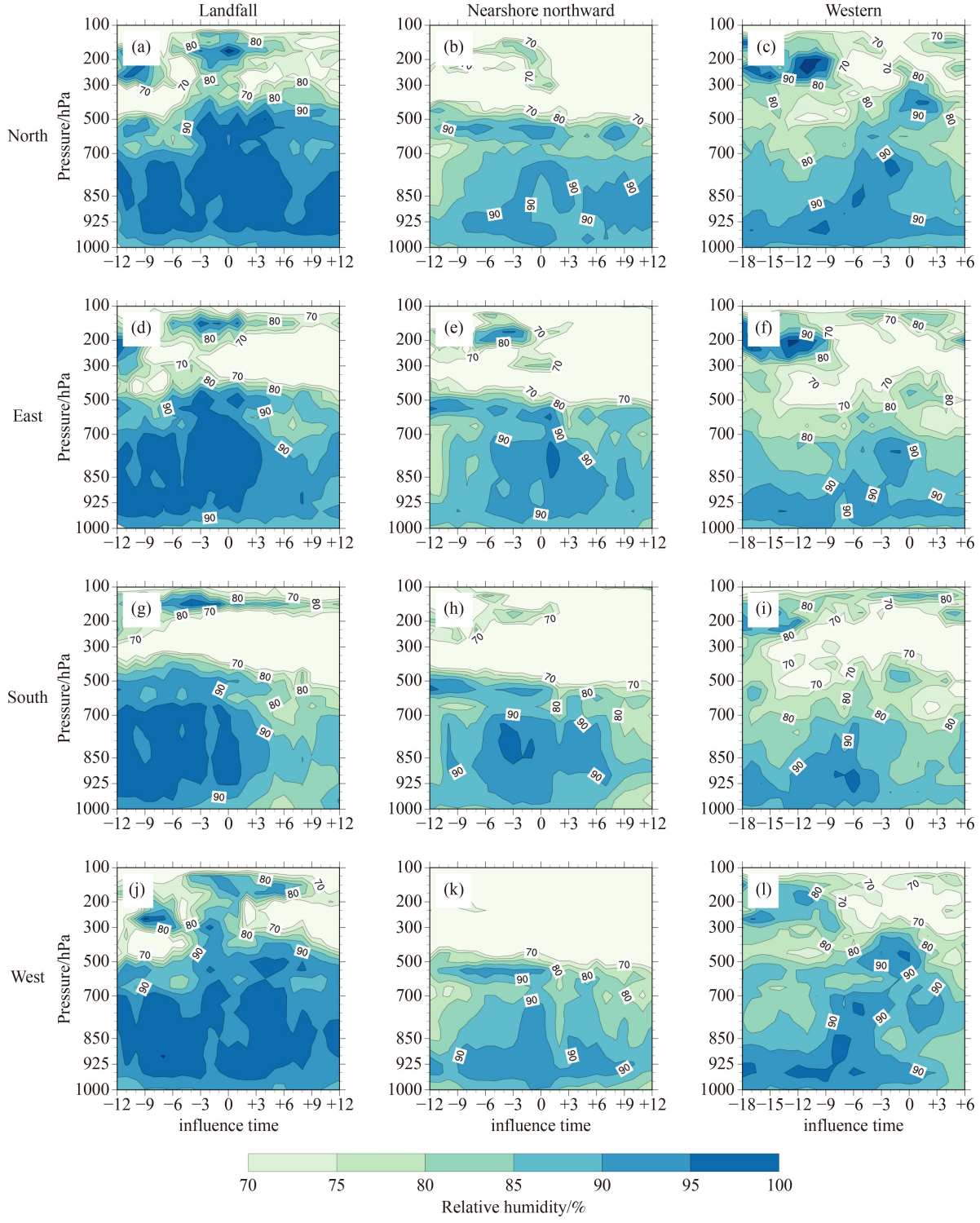

Fig. 5 Time series diagram of relative humidity (color shading, unit: %) at four boundaries of Shanghai under the influence of three types of TC: (a–c): northern boundary; (d–f): eastern boundary; (g–i): southern boundary; (j–l): western boundary. Left column, landfall type; middle column, nearshore northward type; right column, western type.

(Fig. 5(a)). The start time of water vapor saturation at the eastern boundary is earlier than that at northern boundary, but the duration is shorter (Fig. 5(d)). Among the four boundaries, the southern boundary of Shanghai is affected by landfall TCs first, and the thickness of the relative humidity saturation zone at the southern boundary reaches 700 hPa 12 h before the TCs cross the same latitude as Shanghai, but the relative humidity drops rapidly afterward (Fig. 5(g)). The saturation zone thickness at the western boundary reaches 500 hPa at 3–6 h after the TC is at the same latitude (Fig. 5(j)), which lags behind the eastern and northern boundaries. The above analysis shows that the northern boundary has the best relative humidity and longest duration of water vapor saturation when a landfall TC affects Shanghai, whereas the relative humidity condition of the southern boundary is deficient compared to the other boundaries.

When nearshore northward TCs affect Shanghai, the duration of relative humidity over 80% at the lower troposphere of the four boundaries in Shanghai is nearly the same (Figs. 5(b), 5(e), 5(h), 5(k)). Although the high relative humidity zones (> 90%) at the northern and western boundaries lasts a little longer than those at the eastern and southern boundaries of Shanghai, the thickness of the high relative humidity zone is thinner than the counterparts (Figs. 5(b) and 5(k)). At the eastern and southern boundaries, the high relative humidity zone can reach 700 hPa and last about 9 h (Fig. 5(e) and 5(h)). The relative humidity conditions at the eastern and southern boundaries are slightly better than those at other boundaries.

The relative humidity in the boundary layer at the four boundaries is above 85% when western TCs affect Shanghai (Figs. 5(c), 5(f), 5(i), 5(l)). The thickness of the high relative humidity zone (> 90%) at northern boundary reaches 700 hPa from 6 to 3 h before the TC crosses the same latitude as Shanghai (Fig. 5(c)). The vertical distribution of relative humidity at the western boundary is similar to that at the northern boundary, but 2 h ahead (Fig. 5(l)). The high humidity zones at the eastern and southern boundaries maintain for a shorter time than those at the northern and western boundaries, and they are thinner (Figs. 5(f) and 5(i)). These findings indicate that the relative humidity conditions at the western and northern boundaries in Shanghai are better than those of other boundaries in western TCs.

Further comparative analysis of the three TC types shows that when landfall TCs affect Shanghai, the relative humidity condition is the most favorable, and the best relative humidity condition is at the northern boundary. The relative humidity condition is the best when the TC is close to Shanghai during landfall and nearshore northward TCs, but the best relative humidity condition occurs 6–3 h before the TC passes the same latitude as Shanghai during western TCs.

5.2 Water vapor flux and divergence

Water vapor convergence of Landfall TCs is significant at the eastern and northern boundaries of Shanghai. At the northern boundary, horizontal water vapor flux convergence in the boundary layer exceeds 1.5×10^{-6} $g \cdot hPa^{-1} \cdot cm^{-2} \cdot s^{-1}$ from 8 h before the TC reaches the same latitude as Shanghai, and the thickness of the high water vapor flux convergence zone reaches 600 hPa from 3 h before to 3 h after the TC crosses the same latitude (Fig. 6(a)). The convergence intensity of water vapor flux and the thickness and duration of high water vapor flux convergence at the eastern boundary are equivalent to those at the northern boundary, but the start and end times of influence are 1 h earlier than at the northern boundary (Fig. 6(d)). The onset of water vapor flux convergence at the southern boundary in Shanghai is the earliest among the four boundaries, but water vapor convergence at the southern boundary stops when the TC crosses the same latitude as Shanghai (Fig. 6(g)). The onset time of water vapor flux convergence at the western boundary is the latest and the duration of high water vapor flux convergence is the shortest among the four boundaries (Fig. 6(j)). These results suggest that the strongest water vapor flux convergence in Shanghai during landfall TCs is at the northern boundary, followed by the eastern boundary. A stronger easterly wind corresponds to stronger water vapor flux convergence, indicating that sea breezes may be the main contributor to the water vapor supply in Shanghai.

Water vapor convergence at the eastern boundary in Shanghai is greater than that at the other boundaries in nearshore northward TCs. At the eastern boundary, water vapor flux convergence in the boundary layer reaches 10^{-6} $g \cdot hPa^{-1} \cdot cm^{-2} \cdot s^{-1}$ within 3–5 h after the TC passes the same latitude as Shanghai, and the thickness of the high water vapor flux convergence zone reaches 850 hPa. The duration of water vapor convergence is longer than that at the other boundaries (Fig. 6(e)). The convergence intensity of water vapor flux at the southern boundary of Shanghai is second only to that at the eastern boundary, but the water vapor flux convergence at the southern boundary occurs before the TC reaches the same latitude as Shanghai (Fig. 6(h)), whereas water vapor flux convergence at the northern boundary occurs after the TC crosses the same latitude (Fig. 6(b)). Water vapor flux convergence at the western boundary is very weak and almost negligible (Fig. 6(k)). The above findings indicate that the main source of water vapor in Shanghai during nearshore northward TCs is at the eastern boundary.

The water vapor flux convergence during western TCs is concentrated in the period before the TC passes the same latitude as Shanghai (Figs. 6(c), 6(f), 6(i), 6(l)). Water vapor flux convergence is greater and longer at the northern boundary than at the other boundaries, but the intensity is generally about 10^{-6} $g \cdot hPa^{-1} \cdot cm^{-2} \cdot s^{-1}$

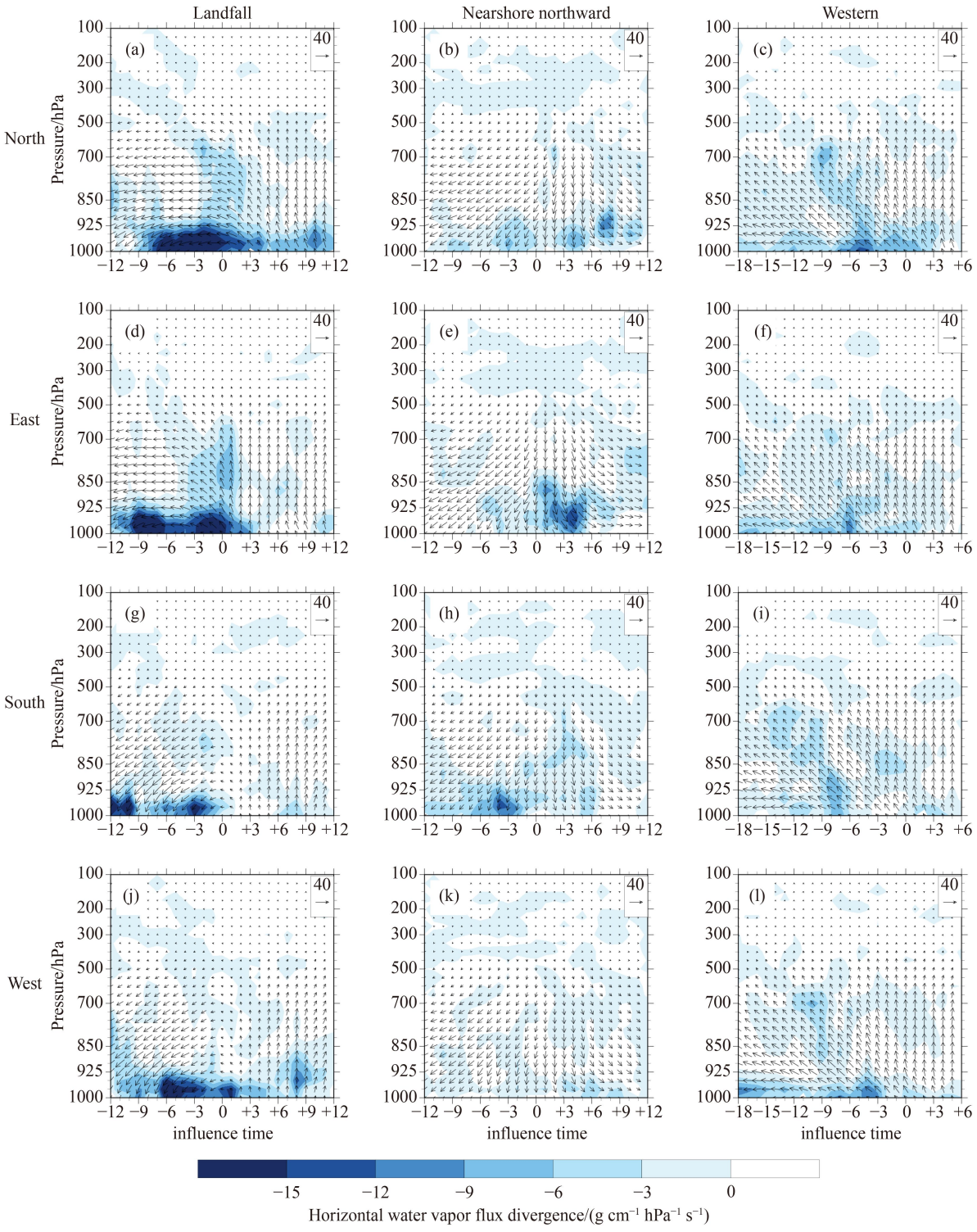

Fig. 6 As in Fig. 5, but for water vapor flux (vector, unit: g·cm^{-1}·hPa $^{-1}$·s^{-1}) and water vapor flux divergence (color shading, unit: 10^{-7} g·cm^{-2}·hPa^{-1}·s^{-1}).

(Fig. 6(c)). In addition, water vapor flux convergence exists when water vapor flux is north-westward. The above results imply that the water vapor supply in Shanghai during western TCs originates from the south-easterly wind and mainly comes from the northern boundary.

The water vapor flux convergence of all three TC types is concentrated within the boundary layer. Further comparison and analysis of the three TC types show that water vapor flux convergence is stronger at all boundaries in Shanghai during landfall TCs compared to nearshore northward and western TCs. During landfall TCs, water

vapor flux convergence is the most significant at the northern boundary, followed by the eastern boundary. The duration of water vapor flux convergence during nearshore northward TCs is shorter than during landfall and western TCs, with water vapor input coming from the eastern boundary. There is stronger water vapor flux convergence at the northern boundary in Shanghai during western TCs, but the difference is not significant compared to the other boundaries.

5.3 Stability and vertical velocity

The vertical lapse rate of the pseudo-equivalent potential temperature above 600 hPa at the four boundaries of Shanghai during landfall TCs is greater than 0, which is convective stable, and below 600 hPa the value is less than 0, which is convective unstable (Figs. 7(a), 7(d), 7(g), 7(j)). When a TC approaches the same latitude as Shanghai, there is an upward movement from 950 to 400 hPa at the four boundaries. The vertical upward motion center at the eastern and northern boundaries is at 600 hPa, which indicates that the convective instability energy of the upward motion originates from below 600 hPa (Figs. 7(a) and 7(d)). At 3 h before reaching the same latitude as Shanghai, upward velocity at the northern boundary exceeds 2.0×10^{-4} hPa·s^{-1}, and the convective unstable layers match the strong upward motion perfectly, which is conducive to precipitation (Fig. 7(a)). The convective unstable conditions and upward motion velocity at the eastern boundary are similar to those at the northern boundary, and their configuration is also similar, but occurs 1 h earlier (Fig. 7(d)). The ascending velocity at the southern and western boundaries is small, and the ascending motion does not match up with the convective unstable layers (Figs. 7(g) and 7(j)). These findings reveal that when landfall TCs affect Shanghai, all boundaries are convective unstable. When a TC is close to the same latitude as Shanghai, only upward velocity at the northern and eastern boundaries reaches 2.0×10^{-4} hPa·s^{-1} or higher, which is favorable to precipitation. The upward motion at the southern and western boundaries is weak and the precipitation dynamic condition is not as favorable as that at the northern and eastern boundaries.

The convective unstable layer at the four boundaries is thin and weak during nearshore northward TCs (Figs. 7(b), 7(e), 7(h), 7(k)). The thickness of the convective unstable layer at the eastern boundary reaches 700 hPa, with a maximum upward motion of more than 5.0×10^{-5} hPa·s^{-1} at 1–3 h after the TC passes the same latitude as Shanghai (Fig. 7(e)). The other boundaries are more stable than the eastern boundary, and their upward motion is negligible (Figs. 7(b), 7(h), 7(k)). The above results show that the stratification conditions and upward motion are favorable for precipitation only at the eastern boundary for a short time when nearshore northward TCs affect Shanghai.

The thickness of the convective instability layer at the four boundaries is relatively thin. The stratification condition is more unstable before the TC crosses the same latitude as Shanghai during western TCs (Figs. 7(c), 7(f), 7(i), 7(l)). The upward motion velocity at the northern, western, and southern boundaries reaches 1.0×10^{-4} hPa·s^{-1} within a short period of time approximately 10 h before the TC crosses the same latitude as Shanghai; however, the unstable convective stratification does not match well with the upward movement, and the precipitation conditions at the western boundary are slightly better (Figs. 7(c), 7(i), 7(l)). The convective instability condition and ascending motion are the weakest at the eastern boundary (Fig. 7(f)). The above results indicate that the stratification condition and upward motion configuration are more favorable to precipitation at the western boundary in Shanghai than at the other boundaries during western TCs.

Further comparative analysis of the three TC types reveals greater convective instability and vertical upward velocity at the four boundaries in Shanghai during landfall TCs than during nearshore northward and western TCs. During landfall TCs, the high convective instability at the northern and eastern boundaries match up well with strong upward motion, which is favorable to precipitation. Only when nearshore northward TCs are at the same latitude as Shanghai, the stratification condition and upward motion configuration at the eastern boundary are favorable for precipitation. During western TCs, the configuration of the stratification condition and upward motion at the western boundary is beneficial for precipitation. Usually, vertical upward velocity within a TC's inner circulation can reach 10^{-2} hPa·s^{-1}, and ERA5 reanalysis data underestimate the extreme upward velocity of TCs.

5.4 Total helicity

For landfall TCs, the total helicity at the northern boundary remains −200 hPa·s^{-2} and higher, with a maximum of −400 hPa·s^{-2}, before the TC is at the same latitude as Shanghai, indicating a strong helicity structure that is favorable for precipitation (Fig. 8(a)). The total helicity at the northern boundary decreases rapidly after the TC crosses the same latitude, indicating a weakening of the helicity structure. The total helicity at the eastern boundary gradually decreases after the TC reaches the maximum (−300 hPa·s^{-2}) at 12 h before it is at the same latitude as Shanghai, and the total helicity at the western boundary is equivalent to that at the eastern boundary, but the time is 3 h earlier (Figs. 8(d) and 8(j)). The total helicity at the southern boundary is small, only about −100 hPa·s^{-2} (Fig. 8(g)). These findings suggest that the high total helicity at the four boundaries are concentrated before TCs cross at the same latitude as Shanghai, indicating that the condition of horizontal wind speed and

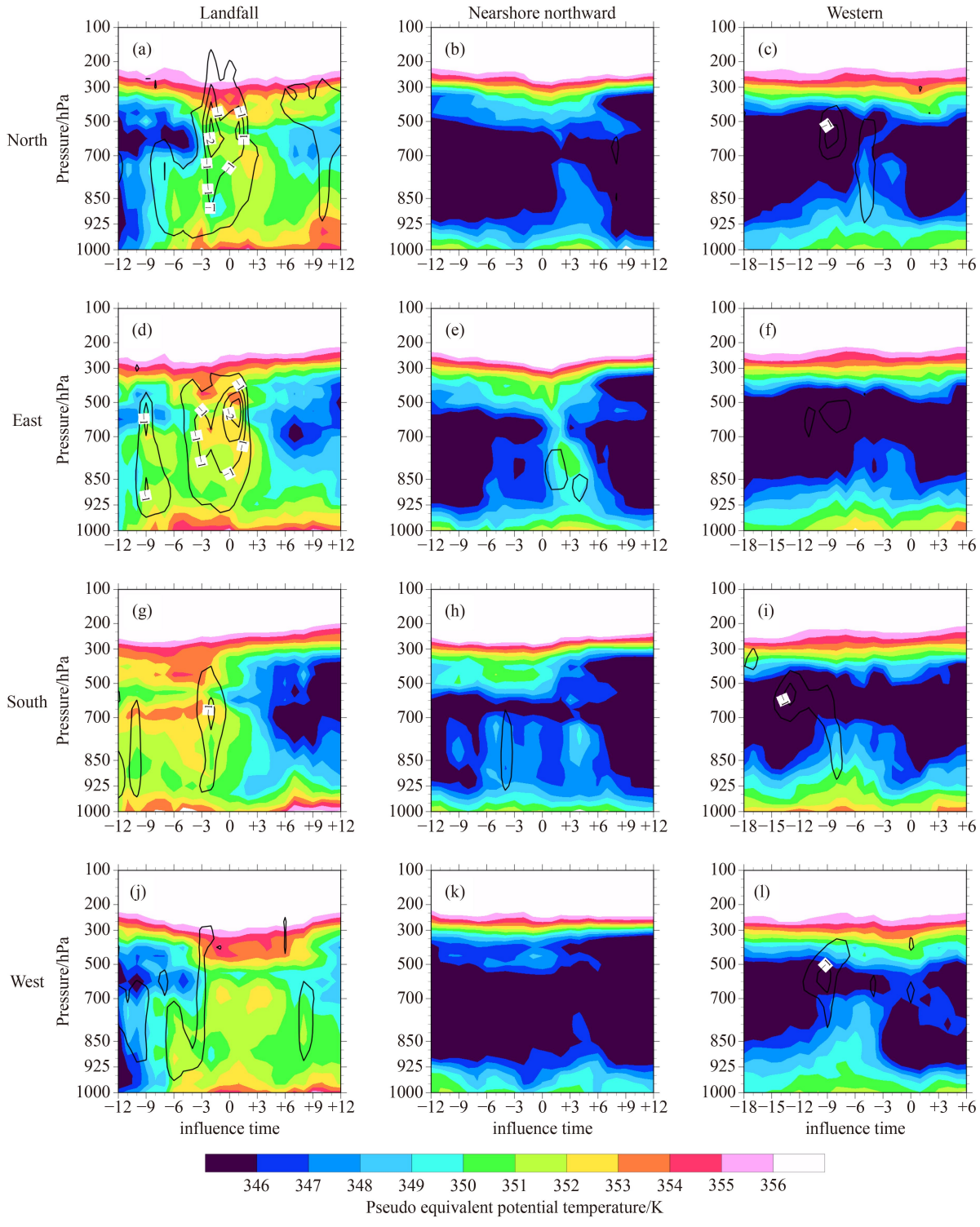

Fig. 7 As in Fig. 5, but for pseudo-equivalent potential temperature (color shading, unit: K) and vertical velocity (solid line, unit: 10^{-4} hPa·s^{-1}).

vertical shear of the horizontal wind is conducive to precipitation. The northern boundary has the best dynamic conditions among the four boundaries.

For nearshore northward TCs, the total helicity at the eastern boundary in Shanghai is the highest and remains high for the longest time (Fig. 8(e)). Total helicity is maintained at −250 hPa·s^{-2} and higher, with a maximum of −400 hPa·s^{-2}, between 12 h before and 7 h after the TC is at the same latitude as Shanghai. The total helicity of the southern and northern boundaries is less than that at the eastern boundary, and the duration of high value is slightly shorter (Figs. 8(b) and 8(h)). The total helicity at

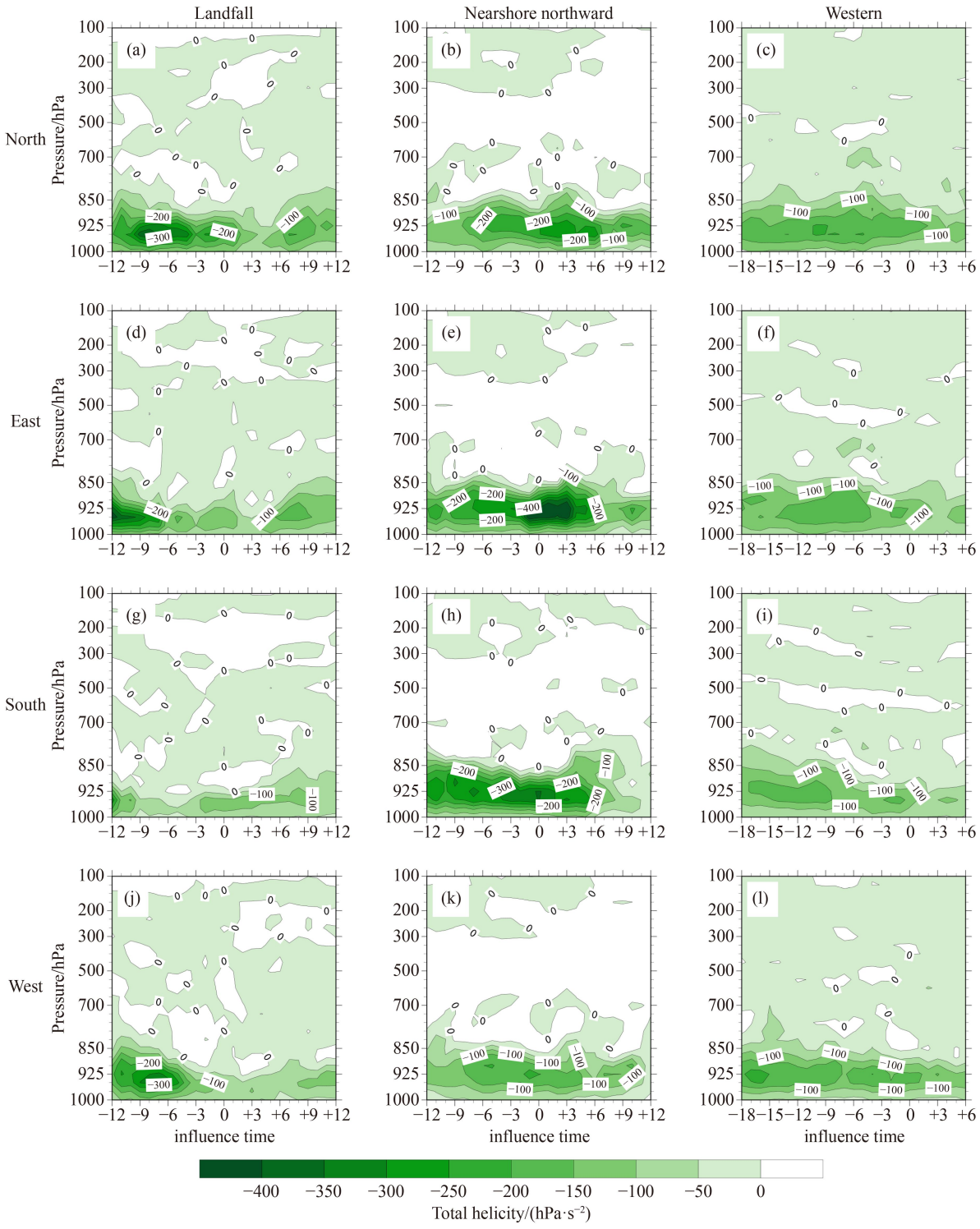

Fig. 8 As in Fig. 5, but for total helicity (color shading, unit: hPa·s^{-2}).

the western boundary is the smallest and the duration is the shortest among the four boundaries (Fig. 8(k)). The total helicity at the four boundaries during nearshore northward TCs reaches the maximum when the TC is at the same latitude as Shanghai, and the eastern boundary has the best dynamic condition among the four boundaries.

The extreme total helicity during western TCs is half of that during landfall and nearshore northward TCs (Figs. 8(c), 8(f), 8(i), 8(l)). The total helicity at the western and northern boundaries remains −100 hPa·s^{-2} and higher, with a maximum of −200 hPa·s^{-2}, before the TC is at the same latitude as Shanghai (Figs. 8(c) and 8(l)). The total helicity at the eastern and southern boundaries is smaller

than that at the western and northern boundaries, and the duration is also shorter (Figs. 8(f) and 8(i)). The total helicity at all four boundaries decreases rapidly after the TC crosses the same latitude as Shanghai. These results imply that favorable dynamic conditions for precipitation during western TCs occurs before the TC is at the same latitude as Shanghai, and the western and northern boundaries have better dynamic conditions than the other boundaries.

Further comparative analysis reveals that the high total helicity zone of the three TC types at all boundaries in Shanghai is concentrated below 850 hPa. In general, the total helicity intensity of nearshore northward TCs is greater than that of landfall and western type TCs, which is related to the strong intensity of nearshore northward TCs.

Under the influence of landfall TCs, the water vapor, dynamic, and convective instability conditions at the northern boundary in Shanghai are the best, followed by the eastern boundary. The main sources of water vapor in Shanghai come from the eastern and northern boundaries, indicating that sea breezes contribute greatly to water vapor. Under the influence of nearshore northward TCs, the main contributions of water vapor, dynamics, and convective instability come from the eastern boundary, and the contributions of other boundaries can be ignored. During western TCs, the dynamics and water vapor conditions at the western and northern boundaries are better, but the advantage is not obvious compared with other boundaries.

6 Summary and discussion

Based on similar tracks from best-track data, TCs that affected and crossed the same latitude as Shanghai from 2007 to 2018 were divided into three types: landfall, nearshore northward, and western TCs. Based on ERA5 reanalysis data, the dynamic synthesis method was used to synthesize TC circulation situations to compare thermal, dynamic, water vapor, and stability conditions within the circulation of TCs during the period when they affect Shanghai. Total helicity diagnostic analysis was also conducted. The conclusions are as follows.

1) There were 11 TCs that affected Shanghai during the study period: four landfall TCs, three nearshore northward TCs, and four western TCs. All TCs caused significant rainfall in Shanghai. When the synthesized TCs are at the same latitude as Shanghai, the average intensity of nearshore northward TCs is the strongest, followed by landfall TCs. The average cumulative rainfall of western TCs is the largest, followed by nearshore northward TCs.

2) A comparison of the circulation patterns of the three TC types reveals that when the synthesized TCs are at the same latitude as Shanghai, all three types in the divergent field at 200 hPa. The difference is that landfall TCs are close to the center of the subtropical high, whereas nearshore northward and western TCs lie between the low trough and the subtropical high. At 500 hPa, the subtropical high pressure during the landfall type is stronger and located farther to north than usual, and there is a high-pressure dam on the north side of the TC, while nearshore northward and western TCs are located on the west side of the subtropical high.

3) A diagnostic analysis of the circulation of the three TC types affecting Shanghai shows that when TCs are at the same latitude as Shanghai, warm advections of all three types are in the northern quadrant at 925 hPa. The difference is that there are better dynamic and water vapor conditions in the western and northern quadrants of landfall and western TCs, whereas nearshore northward TCs have superior dynamic and water vapor conditions in the eastern quadrant. Nearshore northward TCs have stronger intensity of wind field convergence and water vapor flux convergence of the internal circulation than the other two TC types due to the high wind speed.

4) An analysis of the related factors of conditions favorable to precipitation in Shanghai suggests that the dynamic, water vapor, and instability conditions start from the boundary layer for all three TC types. Water vapor, upward motion, and instability conditions of landfall TCs in Shanghai are superior to the other two TC types. The best water vapor, dynamic, and convective instability conditions are at the northern boundary during landfall TCs, and the main sources of water vapor come from the eastern and northern boundaries. During nearshore northward TCs, the main contributor to rainfall comes from the eastern boundary. The better dynamic and water vapor conditions are from the western and northern boundaries during western TCs. In addition, there is a 1−3 h difference between the start and end of the impact of the same type of TCs on different boundaries in Shanghai. Furthermore, the intensity of total helicity of nearshore northward TCs is greater than that of landfall and western TCs, indicating a close relationship between total helicity and TC intensity.

5) A comprehensive analysis of the applicability of ERA5 reanalysis data to TCs affecting Shanghai indicates that from a qualitative point of view, ERA5-based diagnostic analysis can reflect not only the differences in TC circulation in different tracks, but also the temporal, spatial, and intensity differences of the influence of similar tracks on the thermal, dynamic, instability, and water vapor conditions of the four boundaries in Shanghai. However, from a quantitative point of view, ERA5 reanalysis data greatly underestimate the vertical upward velocity within TC circulation.

6) Focusing on the effects of the three TC types on precipitation forecasts in Shanghai, when a TC is close to Shanghai, the greater the wind speed, the better the dynamic conditions. In terms of water vapor conditions,

the conditions at the boundary affected by sea breezes are good. Therefore, for landfall type TCs, attention should be paid to the influence of water vapor input and wind field convergence at the eastern and northern boundaries of Shanghai. For nearshore northward type TCs, attention must be given to the influence of water vapor and dynamic conditions in the eastern part of Shanghai. For western type TCs, due to the close precipitation conditions at each boundary, combined with the effect of ground friction and cold air, the factors affecting precipitation are complex and the predictability of precipitation is poor. These research results can provide scientific and technical support for the operational forecasting of precipitation from TCs in Shanghai.

Acknowledgments This study was supported by the National Natural Science Foundation of China (Grant Nos. 41875059, 41875071, 41875051, 42005077, and U2142206), the Natural Science Foundation of Shanghai Science and Technology Committee (Nos. 21ZR1457700 and 22ZR1456100), and East China Phased Array Weather Radar Application Joint Laboratory.

Competing interests The authors declare that they have no competing interests.

References

Albergel C, Dutra E, Munier S, Calvet J, Munoz-Sabater J, de Rosnay P, Balsamo G (2018). ERA-5 and ERA-Interim driven ISBA land surface model simulations: which one performs better? Hydrol Earth Syst Sci, 22(6): 3515–3532

Belmonte Rivas M, Stoffelen A (2019). Characterizing ERA-Interim and ERA5 surface wind biases using ASCAT. Ocean Sci, 15(3): 831–852

Bian G, Nie G, Qiu X (2021). How well is outer tropical cyclone size represented in the ERA5 reanalysis dataset? Atmos Res, 249: 105339

Bu S, Li Y (2020). Comparative analysis of precipitation distributions of tropical cyclones making landfall in east China. Chin J Atmos Sci, 44(1): 27–38

Chen L, Ding Y (1979). Introduction to Western Pacific Typhoons. Beijing: Science Press (in Chinese)

Dong M, Chen L, Li Y, Lu C (2010). Rainfall reinforcement associated with landfalling tropical cyclones. J Atmos Sci, 67(11): 3541–3558

Feng T, Huang R, Chen G, Wu L, Huang P, Wang L (2013). Progress in recent climatological research on tropical cyclone activity over the western North Pacific. Chin J Atmos Sci, 37(2): 364–382

Feng T, Shen X, Huang R, Chen G (2014). Influence of the interannual variation of cross-equatorial flow on tropical cyclogenesis over the western north Pacific. J Trop Meteorol, 30(1): 11–22

Frank W M (1977). The structure and energetics of tropical cyclone I: storm structure. Mon Wea Rev, 105(9): 1119–1135

Gray W M (1979). Recent advance in tropical cyclone research from rawnsonde analysis. WMO Program on Research in Tropical Meteorology. Department of Atmospheric Science, Colorado State University, Fort Collins, Colorado 80523

Hersbach H, Bell B, Berrisford P, Hirahara S, Horányi A, Muñoz-Sabater J, Nicolas J, Peubey C, Radu R, Schepers D, Simmons A, Soci C, Abdalla S, Abellan X, Balsamo G, Bechtold P, Biavati G, Bidlot J, Bonavita M, Chiara G, Dahlgren P, Dee D, Diamantakis M, Dragani R, Flemming J, Forbes R, Fuentes M, Geer A, Haimberger L, Healy S, Hogan R J, Hólm E, Janisková M, Keeley S, Laloyaux P, Lopez P, Lupu C, Radnoti G, Rosnay P, Rozum I, Vamborg F, Villaume S, Thépaut J N (2020). The ERA5 global reanalysis. Q J R Meteorol Soc, 146(730): 1999–2049

Huang H, Zhao Y, Xun A, Chen J, Zhang W (2021). Causality analysis of difference of heavy rainfall distribution in Fujian caused by typhoons Soulik and Trami along similar tracks in 2013. Torrential Rain Disaster, 40(2): 136–146

Lei X (2001). The precision analysis of the best positioning on WNP TC. J Trop Meteorol, 17(2): 65–70

Lei X, Chen P, Yang Y, Qian Y (2009). Characters and objective assessment of disasters caused by typhoons in China. Acta Meteorol Sin, 67(5): 875–883

Li Y, Chen L, Wang J (2004). The diagnostic analysis of the characteristics of large scales circulation corresponding to the sustaining and decaying of tropical cyclone after its landfall. Acta Meteorol Sin, 62(2): 167–179

Li Y, Chen L, Wang J (2005). Diagnostic study of the sustaining and decaying of tropical cyclones after landfall. Chin J Atmos Sci, 29(3): 482–490

Li Z, Hou Y, Li S, Li J (2021). Characteristics of wave field in the Yellow Sea and the Bohai Sea under the influence of two typical typhoons. Oceanol Limnol Sin, 52(1): 51–65

Lu X, Yu H, Ying M, Zhao B, Zhang S, Lin L, Bai L, Wan R (2021). Western North Pacific tropical cyclone database created by the China Meteorological Administration. Adv Atmos Sci, 38(4): 690–699

Meng X, Guo J, Han Y (2018). Preliminarily assessment of ERA5 reanalysis data. J Marine Meteo, 38(1): 91–99

Ni Z, Wu L, Zhang L (2013). Analysis on forecasting errors and associated circulations of sudden typhoon track changes during 2005–2010. Meteor Mon, 39(6): 719–727

Qian Y, Xu Y, Xu D (2013). Composite analysis on characteristic of tropical cyclone recurvature and landfall over East China Sea. Meteor Mon, 39(12): 1600–1607

Shi J, Xiao F, Mu H, Xu J (2013). Losses assessment of typhoon disaster in Shanghai during 1949–2009. Resour Env Yangtze Basin, 22(7): 952–957

Shou S, Yao X (1995). A diagnostic study of the composite ambient fields of the explosively developing typhoons. Chin J Atmos Sci, 19(4): 487–493

Song J, Wang Y, Wu L (2010). Trend discrepancies among three best track data sets of western North Pacific tropical cyclones. J Geophys Res, 115(D12): D12128

Tan Z, Wu R (1994). Helicity dynamics of atmospheric flow. Adv Atmos Sci, 11(2): 175–188

Xu J (2005). Distribution of wind speed and direction when typhoons influencing Shanghai. Meteor Mon, 31(8): 66–70

Yin H, Wang Y, Zhong W (2016). Characteristics and influence factors of the rapid intensification of tropical cyclone with different tracks

in Northwest Pacific. J Meteorol Sci, 36(2): 54–62

Yu R, Yu H, Duan Y (2013). Relationship between intensity change of tropical cyclone landing in south China and large-scale circulation. Trans Atmos Sci, 36(5): 619–625

Yue C, Guo Y, Shou S, Cao Y (2011). Progress in application study of helicity to severe weathers. Torrential Rain Disaster, 30(2): 107–116

Yue C, Tang Y, Gu W, Han Z, Wang X (2019). Study of urban barrier effect on local typhoon precipitation. Meteor Mon, 45(1): 1611–1620